Hindawi
Mathematical Problems in Engineering
Volume 2020, Article ID 6758261, 9 pages
https://doi.org/10.1155/2020/6758261

Research Article

Design of a 3-RPR Flexure System for Optical Switch Assembly

Guiyue Kou, Mouyou Lin, and Changbao Chu

School of Mechanical and Electrical Engineering, Nanchang Institute of Technology, Nanchang, China

Correspondence should be addressed to Guiyue Kou; yangyanxca@163.com

Received 11 June 2020; Accepted 7 August 2020; Published 26 August 2020

Academic Editor: Jose Merodio

In the MEMS optical switch assembly, the collision is likely to happen between the optical fiber and the U-groove of the chip due to the uncontrollable assembly errors. However, these errors can hardly be completely eliminated by the active control using high precision sensors and actuators. It will cause the large acting force and part damage, which further leads to the assembly failure. To solve this question, this paper presents a novel low-cost three-degree-of-freedom (three-DOF) passive flexure system to adaptively eliminate the planar assembly errors. The flexure system adopts three parallel kinematic chains with a novel 3-RPR structure and has a compact size with a diameter of 125 mm and thickness of 12 mm. A novel eddy current damper with the structure of Halbach array permanent magnets (PMs) is utilized to suppress the adverse mechanical vibration of the assembly system from the background disturbances. Analytical models are established to analyze the kinematic, static, and dynamic performances of the system in detail. Finally, finite element analysis is adopted to verify the established models for optimum design. The flexure system can generate a large deformation of 1.02 mm along the two translational directions and 0.02° along the rotational direction below the yield state of the material, and it has much higher natural frequencies than 200 Hz. Moreover, the large damping force means that the designed ECD can suppress the system vibration quickly. The above results indicate the excellent characteristics of the assembly system that will be applied into the optical switch assembly.

1. Introduction

Precision assembly technique is considered as one of the key technologies in many engineering applications. It plays an important role in the assembly of optical switch, microsensor, microactuator, automotive airbag accelerometer, and other optoelectronic devices [1–4]. Among the above applications, MEMS (microelectromechanical systems) optical switch is a kind of precision system integrated with silicon chip and optical fiber, which is used for switching optical path in the new generation optical communication network. Therefore, it has become a key component of many devices in the optical communication network, such as optical add-drop multiplexer, optic-cross connector, optical exchange, and optical wave router. However, since both the silicon chip and the optical fiber are vulnerable components, the assembly process should consider not only the coupling efficiency of optical fibers but also the damage to these components during assembly. As a result, the assembly of optical switches often requires a complex and precision assembly system, and its packaging cost is very high, which affects the wide application of optical switches. Therefore, in the manufacture of optical switches, the low-cost and high-reliability assembly becomes an unavoidable problem.

In the assembly of optical switch, a microgripper is usually utilized to grasp the optical fiber and place it accurately into the U-groove of the silicon chip. The key to success lies in the assembly system. There are several key design considerations in the design of the assembly system, such as the assembly method, system compactness, and assembly cost. Moreover, the gap between the fiber and the U-groove is only a few micrometers to ensure the optical coupling. During the process of inserting the fiber into U-groove, due to the assembly errors and dimension errors, the collision is likely to happen between the fiber and the U-groove. Large contact force will cause device damage or the fiber slips from the microgripper. Therefore, a small contact force should be guaranteed in the design of the assembly system. On the other hand, for the precision positioning or assembly systems, the vibration is another

considered problem. The external vibration interference can cause the motion of the assembly system to result in the collision between the fiber and the U-groove in the assembly process or the rotation of the fiber in the U-groove after the assembly. Thus, the vibration suppression of the system is also the prerequisite to ensure the assembly success in the design of the assembly system.

The successful assembly of the optical switch mainly depends on the elimination of the assembly errors between the objects to a great extent. According to the different methods of processing and eliminating assembly errors, there are two main forms suitable for assembly system, i.e., the active and passive methods [5–7]. The active assembly system usually adopts a high-resolution microscope and multiaxis microforce sensor to detect the assembly state and contact force and further eliminates the assembly errors by actively controlling the multi-DOF precise motion mechanism. For the passive microassembly, as the name suggests, it adopts the elastic deformation of special assembly mechanism to passively eliminate assembly errors. It belongs to an adaptive assembly method without any actuators or sensors. Therefore, if considering the factors of the system cost and structural compactness, the passive one is more suitable for optical switch assembly.

Compared with the conventional rigid mechanism, the flexure mechanism has been widely used in the precision assembly system since it has the advantage of zero backlash, free assembly, zero friction, etc. [8, 9]. Due to the deformation of the material, the flexure mechanism possesses a smaller range of motion but with higher motion precision relative to the rigid mechanism. So far, a lot of research on passive microassembly based on the flexure mechanism has been reported in the literature. A passive error compensator based on elastic shear pad produced by ATI company, which can compensate the multidirectional assembly errors, has been widely used in the peg-in-hole assembly system [10]. Lee presented a novel variable remote center compliance (RCC) with modified elastic shear pad for robot assembly, which can significantly improve the error compensation capability [11]. Walsh designed a six-DOF RCC mechanism based on the Stewart platform, which is made of the flexure-beam hinge to realize the error compensation in the six directions of the space [12]. However, the stiffness of the mechanism in all directions is relatively small in order to pursue a large deformation, which is easy to cause the mechanical vibration. Chen and Lin proposed a three-DOF flexure assembly system for MEMS optical switch assembly [13]. In order to avoid the large mechanical vibrations, the system stiffness along three planar motion directions are very large, which results in a small error compensation range.

For the flexure-based assembly system, the stiffness of the flexure mechanism should be much lower for a large error compensation range. However, it will cause the adverse mechanical vibration. Therefore, it is necessary to design a damper for the vibration suppression of the low-stiffness assembly system. Up to now, various dampers have been developed to suppress the mechanical vibration, i.e., tuned mass damper, viscous damper, eddy current damper (ECD), etc. [14–16]. It is noted that the ECD is a noncontact electromagnetic damper, where the eddy current can be induced in the moving conductor by the relative movement between the conductor and the fixed static field or by changing the magnetic field strength in the fixed conductor. The vibration energy is finally dissipated through the heat energy of the conductor. Therefore, the passive ECD is very suitable for the vibration suppression of flexure assembly system in comparison with other dampers. Now, the passive ECD has been successfully used in the many applications of braking system, precision machining, and automobile suspension system [17–19]. For example, Sodano developed a passive ECD to suppress the vibration of a cantilever beam. Fan proposed a novel ECD for finish machining of assembly interfaces of large vertical tail. Teshima analyzed the effect of ECDs on the vibrational performances in the superconducting levitations. Sung utilized the passive ECD to enhance the positioning accuracy of a linear air-bearing motion stage.

This paper presents a low-cost flexure assembly system, utilizing a three-DOF flexure mechanism based on the 3-RPR structure and a passive ECD to guarantee a large error compensation range with negligible mechanical vibration. In the remainder of this paper, the flexure assembly system is firstly introduced in detail in Section 2. The analytical models about the kinematic, static, and dynamic performance are derived in Section 3. Afterwards, finite element analysis is conducted to verify the theoretical modeling in Section 4.

2. Assembly System Description

2.1. Optical Switch Assembly. Figure 1 shows the optical switch assembly. It can be seen that the fiber is held by a gripper or a vacuum head and inserted into the U-groove of a silicon chip. During the overall assembly, the assembly errors from the relative positioning errors between the fiber and the U-groove can result in a large contact force. Once the contact force exceeds the allowable maximum contact force, the switch or the fiber will be damaged. If the optical switch is placed at a passive flexure mechanism, the contact force will drive the mechanism to move along the direction of decreasing assembly error.

2.2. Mechanical Structure. As shown in Figure 2, an assembly system is designed for the optical switch assembly. It mainly includes two critical components, i.e., three-DOF flexure mechanism and a passive ECD. It can be seen that the flexure mechanism has three identical parallel kinematic chains that suspend the output end from the three sides. Each chain includes two revolute flexure joint denoted by R and a prismatic flexure joint denoted by P. It is obvious that the flexure mechanism belongs to the class of 3-RPR parallel kinematic mechanisms, which can provide the planar three-DOF motions (x, y, and θ). The optical switch is placed on the upper surface of the output end. Thus, the developed passive flexure mechanism can be utilized to eliminate the planar assembly errors in the

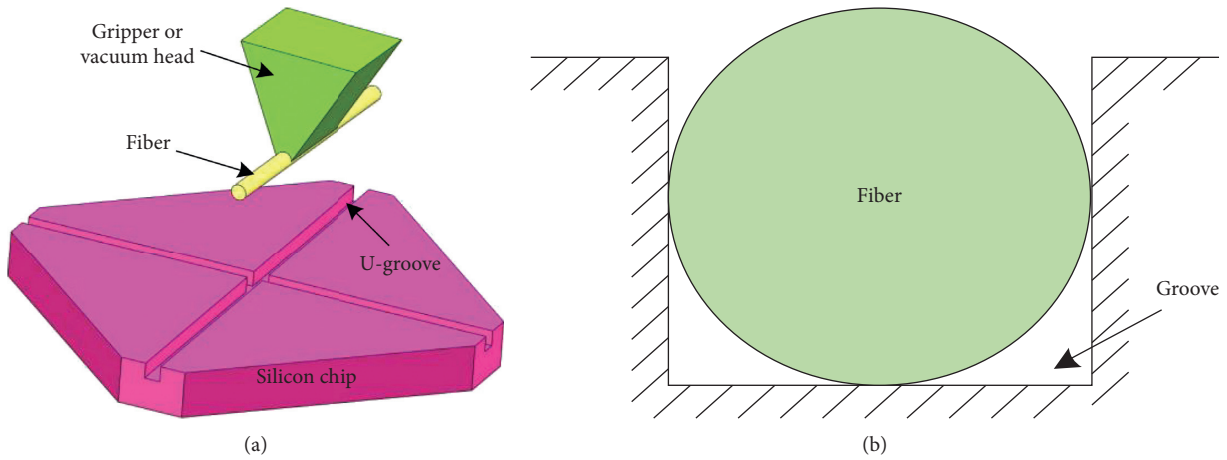

Figure 1: Optical switch assembly (a) before and (b) after fiber insertion.

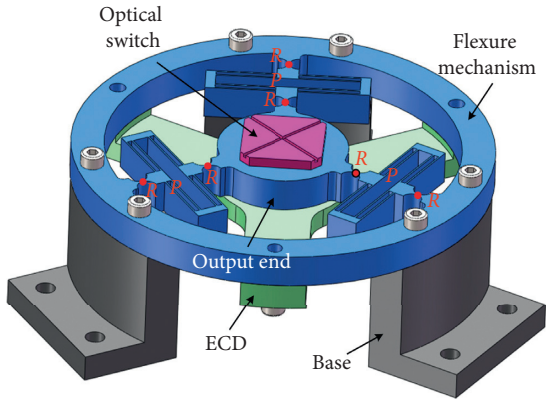

Figure 2: Mechanical structure of an optical switch assembly.

optical switch assembly. In order to obtain a large error compensation range, the stiffness of the flexure mechanism should be relatively small. The intersection of three motion chains, i.e., the geometric center of the flexure mechanism, is the remote center of compliance, where the stiffness matrix is a diagonal matrix.

As shown in Figure 2, in order to suppress vibration of the assembly system, a passive ECD is mounted on the rear side of the flexure mechanism, which adopts the structure of single-layer PMs and a conductor. The conductor is attached to the lower surface of the output end. In the ECD, eight PMs are arranged in Halbach array with closed and continuous magnetic flux path as shown in Figure 3. Compared with other PM arrays, the Halbach array has the highest magnetic flux density, which can enhance the damping force and facilitate the compact design of the system. The conductor is close to the reinforcing side of the PM magnetic field density, i.e., the upper surface of the PM array as shown in Figure 3. Note that the materials of PM and conductor are selected as NdFeB N52 and copper for high magnetic flux density and high electrical conductivity, respectively. Moreover, the damping ratio of the ECD can be adjusted by changing the clearance between the conductor and the PM array.

3. System Modeling

3.1. Kinematics Analysis. According to the pseudorigid body model (PRBM) method [20], each flexure joint can be equivalent to be a rigid joint with a spring stiffness. The kinematic model of the flexure mechanism is shown in Figure 4. Kinematics analysis refers to the relationship between each joint variable and the output motion. The joint variables of the ith chain are presented as $\begin{bmatrix} q_1^i & j_2^i & \psi_3^i \end{bmatrix}$ and the displacements of the geometric center O of the output end are denoted as $\begin{bmatrix} x & y & \theta \end{bmatrix}$ with respect to the fixed base. The velocity of the output end can be related to the joint velocity of the ith chain by the Jacobian matrix J, i.e.,

$$\begin{bmatrix} \dot{q}_1^i \\ \dot{j}_1^i \\ \dot{\psi}_1^i \end{bmatrix} = J \begin{bmatrix} \dot{x} \\ \dot{y} \\ \dot{\theta} \end{bmatrix} = \begin{bmatrix} J_{11} & J_{12} & J_{13} \\ J_{21} & J_{22} & J_{23} \\ J_{31} & J_{32} & J_{33} \end{bmatrix} \begin{bmatrix} \dot{x} \\ \dot{y} \\ \dot{\theta} \end{bmatrix}, \tag{1}$$

where J_{ij} is the kinematic influence coefficients of the output motion on each flexure joint. The elements of the Jacobian matrix can be derived by the velocity analysis as follows:

$$J = \begin{bmatrix} -S(30^\circ - j_1 - \theta) & C(30^\circ - j_1 - \theta) & -bC(j_1 + \theta) \\ \dfrac{C(30^\circ - j_1 - \theta)}{q_1} & \dfrac{S(30^\circ - j_1 - \theta)}{q_1} & \dfrac{bS(j_1 + \theta)}{q_1} \\ \dfrac{C(30^\circ - j_1 - \theta)}{q_1} & \dfrac{S(30^\circ - j_1 - \theta)}{q_1} & \dfrac{(bS(j_1 + \theta) + q)}{q_1} \end{bmatrix}, \tag{2}$$

where b is the distance from the point O to the point B_i as shown in Figure 3.

3.2. Static Analysis. According to the formulation [21], the stiffness of the revolute flexure joint can be expressed as

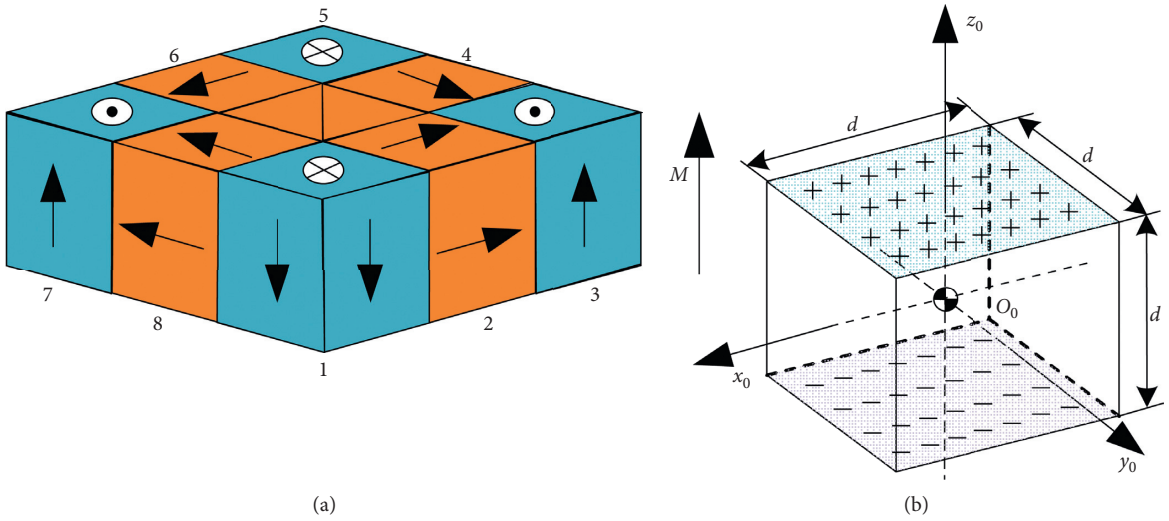

Figure 3: Halbach PM array of the ECD. (a) 3D isometric view and (b) parameter definition of one PM.

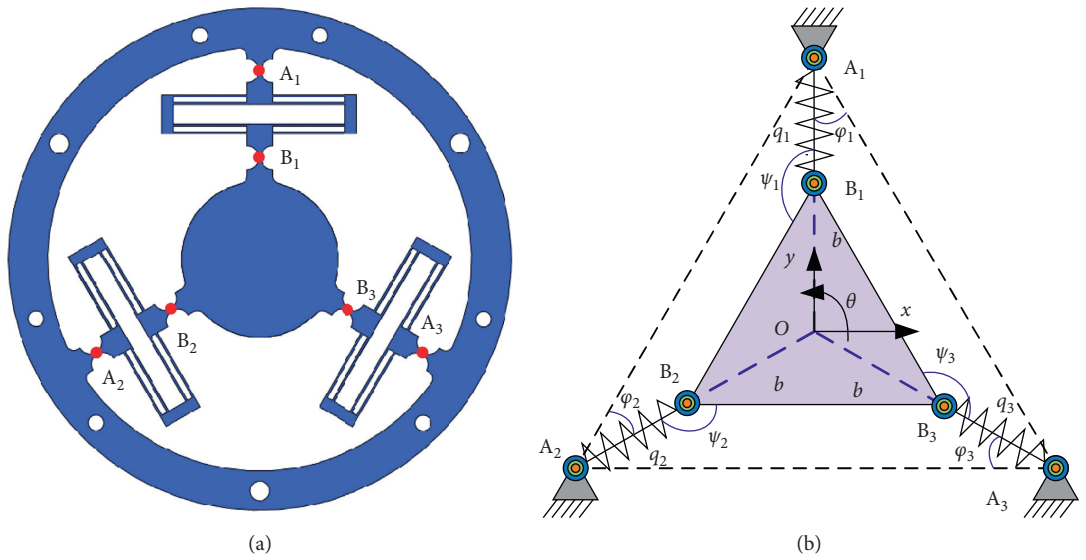

Figure 4: (a) CAD model and (b) kinematic model of the flexure mechanism.

$$K_A = K_B = \frac{2Eht^{2.5}}{9\pi r^{0.5}}, \tag{3}$$

where E is the elastic modulus of the material and h, t, and r are the width, minimum thickness, and radius of the revolute flexure joint, respectively.

It is observed that the prismatic flexure joint has eights beams suffering from the same deformation with a combined force F and moment M (see Figure 5). Considering the boundary condition, the following relationship can be obtained:

$$F = \frac{2M}{l},$$
$$\delta = \frac{Fl^3}{12EI}. \tag{4}$$

Then, the stiffness of the prismatic flexure joint at the output direction is derived as

$$K_P = \frac{F_x}{2\delta} = \frac{4F}{2\delta} = \frac{24EI}{l^3}. \tag{5}$$

Thus, the output stiffness matrix of the platform can be expressed as

$$K = \mathrm{diag}\left(K_x \;\; K_y \;\; K_\theta \right), \tag{6}$$

where $K_x = K_y = (3/2)(K_P + ((K_A + K_B)/q))$ and

$$K_\theta = 3K_P b^2 \cos^2(j+\theta) + \frac{3K_A}{q^2} b^2 \sin^2(j+\theta) + \frac{3K_B}{q^2}(a\sin(j+\theta) + q)^2. \tag{7}$$

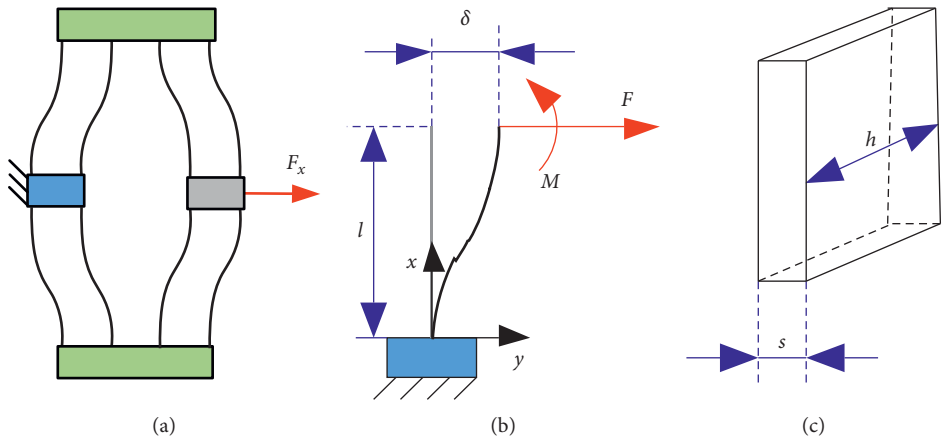

Figure 5: (a) Deformation of the prismatic flexure joint and dimensions of (b) one beam and (c) cross section.

3.3. Dynamic Analysis. In the eddy current damping, the static magnetic field comes from a single-layer Halbach PM array as shown in Figure 3. In order to accurately compute the magnetic field of any point in space, the magnetic surface charge method is adopted to compute the magnetic field density distribution of the developed ECD, where the magnetic fields of all PMs are included in the modeling. The magnetic field density from the magnetic charge surface of one PM is expressed as [22]

$$B({}^{L}r) = \frac{B_r}{4\pi}\sum_{i=0}^{1}\sum_{j=0}^{1}\sum_{k=0}^{1}(-1)^{i+j+k}\begin{pmatrix}\ln(R-T)\\ \ln(R-S)\\ \tan^{-1}(ST/RU)\end{pmatrix}, \quad (8)$$

where B_r presents the remanent flux density of the selected PM.

It is noted that any position ${}^{L}r$ in the local coordinate system can be transformed into ${}^{G}r$ in the global coordinate system as follows:

$${}^{G}r = R_m \cdot {}^{L}r + {}^{G}P_m, \quad (9)$$

where R_m and ${}^{G}P_m$ present the rotation matrix and relative position of the local coordinate system in the global coordinate system.

Then, the magnetic field density of one PM in the global coordinate system is derived as

$$B_m({}^{G}r) = R_m \cdot B_m\left(R_m^{-1}\left({}^{G}r - {}^{G}P_m\right)\right). \quad (10)$$

By applying this transformation relatioship to eight PMs, and meanwhile based on the superposition principle, the magnetic flux density distribution of the PM array in the developed ECD can be written as

$$B({}^{G}r) = \sum_{m=1}^{8} B_m({}^{G}r). \quad (11)$$

Taking the x-axis or y-axis mechanical vibration for example, due to the relative motion between the constant magnetic field and the moving copper conductor, the eddy current density is given as

$$J = \alpha\sigma(v \times B) = \alpha\sigma v\left(-{}^{G}B_z\, j + {}^{G}B_y k\right), \quad (12)$$

where α is the correction factor considering the finite conductor size and the surface Coulomb charge [23], σ describes the conductive coefficient of the moving conductor, and v is the conductor velocity along the x- or y-axis.

Based on Lorentz's law, the electromagnetic force of the conductor is induced as

$$\begin{aligned} F_e &= \int_V (J \times B)\mathrm{d}V \\ &= \alpha\sigma v i\int_V\left[\left(-{}^{G}B_y^2 - {}^{G}B_z^2\right)i + {}^{G}B_x\,{}^{G}B_y j + {}^{G}B_x\,{}^{G}B_z k\right]\mathrm{d}V. \end{aligned} \quad (13)$$

Therefore, the damping force along the x-axis or y-axis can be obtained as

$$F_d = -\alpha\sigma v\int_V\left({}^{G}B_y^2 + {}^{G}B_z^2\right)\mathrm{d}V. \quad (14)$$

Furthermore, the damping coefficient of the designed ECD can be written as

$$c = \alpha\sigma\int_V\left({}^{G}B_y^2 + {}^{G}B_z^2\right)\mathrm{d}V. \quad (15)$$

Similarly, the damping coefficient along the z-axis can be also obtained, which is omitted for brevity here.

Figure 6 shows the dynamic model of the flexure mechanism. The damping coefficients are mainly from the passive ECD along the x, y, and θ directions. The generalized coordinates of the system are selected as $q(t) = \begin{bmatrix} x & y & \theta \end{bmatrix}^T$ and the external force $F(t) = \begin{bmatrix} F_x e^{j\omega t} & F_y e^{j\omega t} & M e^{j\omega t} \end{bmatrix}^T$ is exerted on the output end. According to Lagrange's equation, the dynamic equation of the overall assembly system can be derived as

$$M\ddot{q}(t) + K\dot{q}(t) + Cq(t) = Fq(t), \quad (16)$$

where the mass, stiffness, and damping matrices can be expressed as

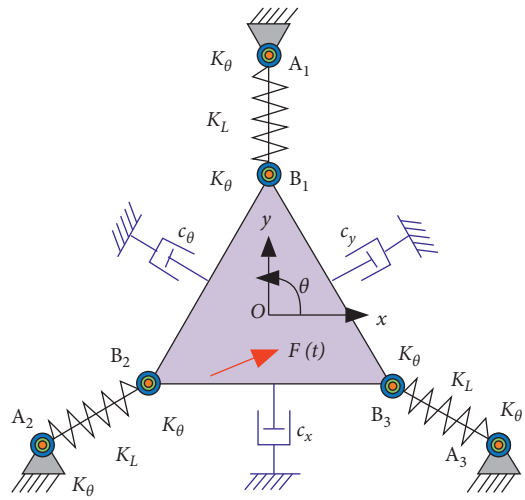

Figure 6: Dynamic model of the flexure mechanism.

Table 1: Parameters of the flexure assembly system.

Parameter	Value
Dimensions of the revolute flexure joint ($r \times h \times t$)	$3 \times 10 \times 0.5\ \text{mm}^3$
Dimensions of the prismatic flexure joint ($l \times h \times s$)	$18.5 \times 10 \times 0.5\ \text{mm}^3$
Dimensions of the PM ($d \times d \times d$)	$5 \times 5 \times 5\ \text{mm}^3$
Dimensions of the conductor ($l \times l \times t$)	$25 \times 25 \times 1.5\ \text{mm}^3$

$$\begin{aligned} M &= \text{diag}\{m_x \;\; m_y \;\; m_\theta\}, \\ C &= \text{diag}(c_x \;\; c_y \;\; c_\theta), \\ K &= \text{diag}(K_x \;\; K_y \;\; K_\theta). \end{aligned} \tag{17}$$

4. Finite Element Analysis

In order to test the performance of the designed flexure assembly system, finite element simulations are conducted with ANSYS 19.0. The structural parameters of the assembly system are shown in Table 1. The main material specifications of the flexure mechanism are Young's modulus of 71.7 GPa, yield strength of 503 MPa, and Poisson's ratio of 0.33. Moreover, the material specifications of the PM are remanent flux density of 1.45 T, conductive coefficient of the conductor of 5.8×10^7 S/m, and conductor permeability of $4\pi \times 10^{-7}$ H/m.

First, the static characteristic of the flexure mechanism is evaluated by applying a force or torque at the output end. The deformation results and stress distribution of the flexure mechanism are shown in Figure 7. Considering that the identical characteristics occur at the x-axis and y-axis, only the x-axis static analysis is performed. Under the force of 50 N along the x-axis, the maximum displacement of the flexure mechanism is about 1.02 mm, but the maximum stress is 435.4 MPa and less than the yield strength of the material. Moreover, the maximum angle displacement is about 0.02° with the stress of 419 MPa for a given torque of 2 N·m. It can be seen that the developed flexure mechanism has a large error compensation range, which can satisfy the requirements of almost all optical switch assembly.

Second, the modal analysis is conducted to evaluate the dynamic characteristic of the flexure mechanism. As shown in Figure 8, it is seen that the first mode shape is attributed to the translation along the x-axis with the frequency of 200.17 Hz whereas the second one indicates the y-axis translation with the frequency of 200.19 Hz. The third mode (371.25 Hz) is caused by the rotational motion of the flexure mechanism. Moreover, the fourth frequency (761.39 Hz) of the local vibration mode is over twice higher than the rotational frequencies. Therefore, the designed flexure mechanism has two translational DOFs and a rotational DOF.

The finite element model of the ECD is established using ANSYS Maxwell 19.0. The flux density distribution is given as shown in Figure 9. It is seen that the Halbach array can enhance the z-axis component of the flux density distribution but the other components are basically weakened, which can improve the eddy current damping. In order to evaluate the damping characteristic, taking the x-axis damping motion as an example, the relationship between the damping force and the conductor velocity is obtained as shown in Figure 10 through several simulations. It is observed that the damping force is linearly related to the conductor velocity. Moreover, the damping coefficient varies with the clearance between the PM array and the conductor as shown in Figure 11; i.e., the smaller the clearance, the greater the damping coefficient.

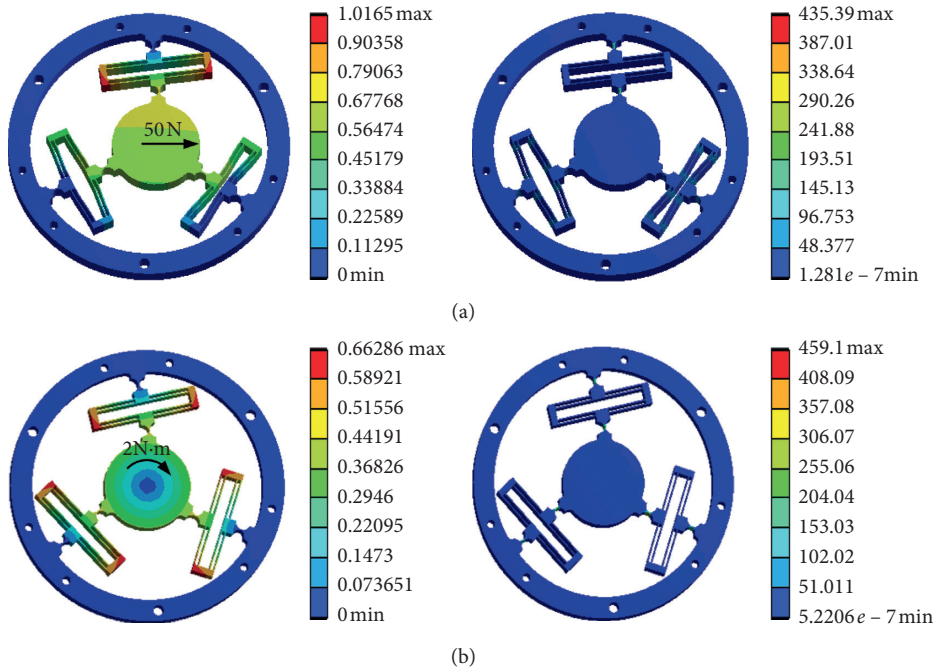

Figure 7: Static analysis results. Deformed shapes and stress distribution (a) in the x direction and (b) in the θ_z direction.

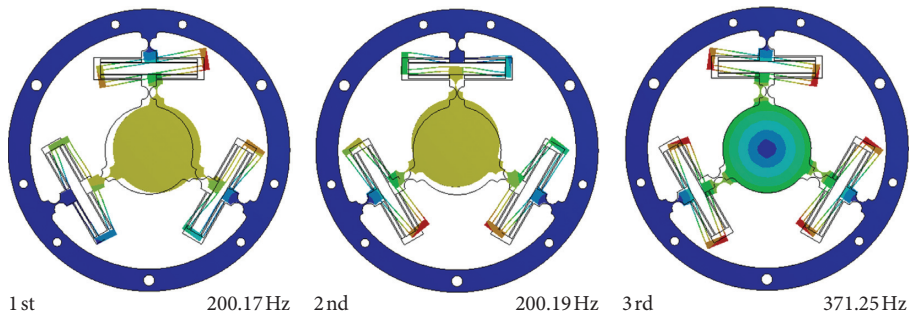

Figure 8: The first three resonant modes of the flexure mechanism.

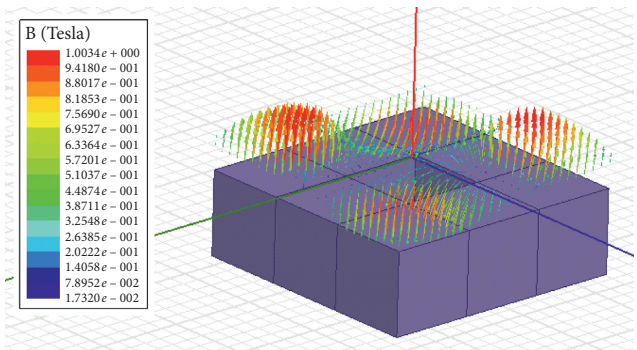

Figure 9: Flux density distribution of the designed ECD.

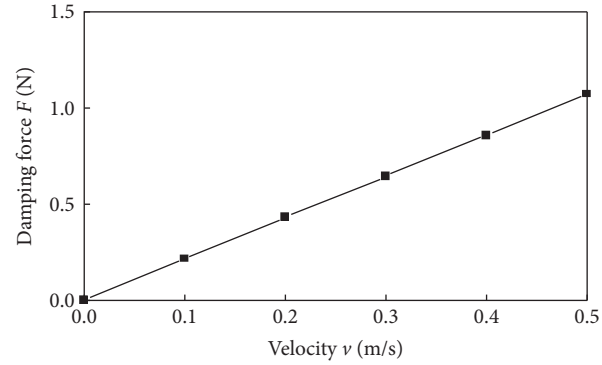

Figure 10: Damping force vs. the conductor velocity.

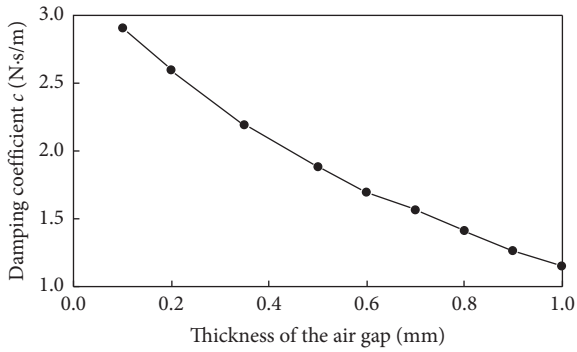

Figure 11: Damping coefficient vs. thickness of air gap.

5. Conclusion

This paper proposes a low-cost passive method for the optical switch assembly. The key component of the assembly system is a 3-RPR flexure-based mechanism, which has a planar three-DOF motion. In order to eliminate the large assembly error, the developed system is designed to have low stiffness. Since low stiffness can cause the adverse mechanical vibration, an eddy current damper is integrated into the system. Analytical models are established to predict the motion characteristic of the flexure-based mechanism and the damping characteristic of the damper, respectively. Finally, finite element analysis is conducted to verify the effectiveness of mechanism design. The simulation results show that the system has a large error compensation range of 1.02 mm along two translational directions and 0.02° along the rotational direction. Moreover, the developed damper has a large damping force due to the Halbach array of the permanent magnet.

Data Availability

The data used to support the findings of this study are included within the article.

Conflicts of Interest

The authors declare that there are no conflicts of interest regarding the publication of this paper.

Acknowledgments

This work was supported by the National Natural Science Foundation of China under Grant no. 51567018, Science and Technology Research Project of Jiangxi Province Education Department under Grant no. GJJ151131, and Natural Science Foundation of Jiangxi Province under Grant nos. 20161BAB206119 and 20161BAB216105.

References

[1] S. Chen, W. Chen, J. Liu, and W. Chen, "A novel 5-DOF flexure-based passive alignment stage for microassembly system," in *Proceedings of the 19th IEEE International Conference on Nanotechnology*, pp. 173–178, Macau, June 2019.

[2] C. R. Giles, V. Aksyuk, B. Barber, R. Ruel, L. Stulz, and D. Bishop, "A silicon MEMS optical switch attenuator and its use in lightwave subsystems," *IEEE Journal of Selected Topics in Quantum Electronics*, vol. 5, no. 1, pp. 18–25, 1999.

[3] H. G. Teo, A. Q. Liu, J. Singh, M. B. Yu, and T. Bourouina, "Design and simulation of MEMS optical switch using photonic bandgap crystal," *Microsystem Technologies*, vol. 10, no. 5, pp. 400–406, 2004.

[4] M. Ghafarian, B. Shirinzadeh, A. Al-Jodah, T. K. Das, W. Wei, and T. Shen, "Modeling and prototype experiment of a monolithic 3-PUU parallel micromanipulator with nanoscale accuracy," *Smart Materials and Structures*, vol. 29, no. 7, p. 075023, 2020.

[5] A. N. Ds, D. O. Popa, and H. E. Stephanou, "Automated microassembly using precision using hybrid control," in *Proceedings of the IEEE International Conference on Robotics and Automation*, pp. 4106–4112, Anchorage, AK, USA, May 2010.

[6] G. Yang, "Scale-based integrated microscopic computer vision techniques for micromanipulation and microassembly," Ph.D. thesis, University of Minnesota, Minneapolis, MN, USA, 2003.

[7] D. O. Popa, R. Murthy, and A. N. Das, "M^3-Deterministic, multiscale, multirobot platform for microsystems packaging: design and quasi-static precision evaluation," *IEEE Transactions on Automation Science and Engineering*, vol. 6, no. 2, pp. 345–361, 2009.

[8] H. Huang, Z. Xu, J. R. Wang, and J. S. Dong, "A low frequency operation high speed stick-slip piezoelectric actuator achieved by using a L-shape flexure hinge," *Smart Materials and Structures*, vol. 29, no. 6, p. 065007, 2020.

[9] Q. Xu, "Design of a large-range compliant rotary micropositioning stage with angle and torque sensing," *IEEE Sensors Journal*, vol. 15, no. 4, pp. 2419–2430, 2015.

[10] http://www.ati-ia.com/products/compliance/Compensator_main.aspx.

[11] S. Lee, "Development of a new variable remote center compliance (VRCC) with modified elastomer shear pad (ESP) for robot assembly," *IEEE Transactions on Automation Science and Engineering*, vol. 2, no. 2, pp. 193–197, 2005.

[12] C. J. Walsh, "Analysis of remote center of compliance device based on Stewart platforms," Ph.D. thesis, Massachusetts Institute of Technology, Cambridge, MA, USA, 2010.

[13] W. Chen and W. Lin, "Fiber assembly of MEMS optical switches with U-groove channels," *IEEE Transactions on Automation Science and Engineering*, vol. 5, no. 2, pp. 207–215, 2008.

[14] W.-H. Lin and A. K. Chopra, "Earthquake response of elastic SDF systems with non-linear fluid viscous dampers," *Earthquake Engineering & Structural Dynamics*, vol. 31, no. 9, pp. 1623–1642, 2002.

[15] J. Lu, Z. Zhan, X. Liu, and P. Wang, "Numerical modeling and model updating for smart laminated structures with viscoelastic damping," *Smart Materials and Structures*, vol. 27, no. 7, p. 075038, 2018.

[16] T. Ransom, A. Honeycutt, and T. Schmitz, "A new tunable dynamics platform for milling experiments," *Precision Engineering*, vol. 44, pp. 252–256, 2016.

[17] J.-H. Kim, Y.-G. Lee, and C.-G. Kim, "An experimental study on a new air-eddy current damper for application in low-frequency accelerometers," *Journal of Mechanical Science and Technology*, vol. 29, no. 9, pp. 3617–3625, 2015.

[18] W. Fan, L. Zheng, W. Li, X. Zhao, L. Wang, and Y. Yang, "Eddy current-based vibration suppression for finish

machining of assembly interfaces of large aircraft vertical tail," *Journal of Manufacturing Science and Engineering*, vol. 141, no. 7, p. 071012, 2019.

[19] E. Sung, C. Seo, H. Song et al., "Design and experiment of noncontact eddy current damping module in air bearing guided linear motion system," *Advances in Mechanical Engineering*, vol. 11, no. 8, pp. 1–11, 2019.

[20] L. L. Howell, *Compliant Mechanisms*, Wiley, New York, NY, USA, 2001.

[21] N. Lobontiu, *Compliant Mechanisms: Design of Flexure Hinges*, CRC Press, Boca Raton, FL, USA, 2002.

[22] K. J. W. Pluk, T. A. van Beek, J. W. Jansen, and E. A. Lomonova, "Modeling and measurements on a finite rectangular conducting plate in an eddy current damper," *IEEE Transactions on Industrial Electronics*, vol. 61, no. 8, pp. 4061–4072, 2014.

[23] J.-S. Bae, M. K. Kwak, and D. J. Inman, "Vibration suppression of a cantilever beam using eddy current damper," *Journal of Sound and Vibration*, vol. 284, no. 3–5, pp. 805–824, 2005.